IEEE Access
Multidisciplinary | Rapid Review | Open Access Journal

Received 7 October 2022, accepted 19 October 2022, date of publication 7 November 2022, date of current version 16 November 2022.

Digital Object Identifier 10.1109/ACCESS.2022.3220237

APPLIED RESEARCH

Finite-Time Output Control for Uncertain Robotic Manipulators With Time-Varying Output Constraints

DUC THIEN TRAN[1], (Member, IEEE), HOAI VU ANH TRUONG[2], MAOLIN JIN[3], (Senior Member, IEEE), AND KYOUNG KWAN AHN[2], (Senior Member, IEEE)

[1]Department of Automatic Control, Ho Chi Minh City University of Technology and Education, Ho Chi Minh City 700000, Vietnam
[2]School of Mechanical Engineering, University of Ulsan, Ulsan 44610, South Korea
[3]Human-Centered Robotics Center, Korea Institute of Robotics and Technology Convergence (KIRO), Pohang 37666, South Korea

Corresponding author: Kyoung Kwan Ahn (kkahn@ulsan.ac.kr)

This work was supported in part by the Basic Science Program through the National Research Foundation of Korea (NRF) funded by the Ministry of Science and Information and Communications Technology (ICT), South Korea, under Grant NRF 2020R1A2B5B03001480; and in part by the Regional Innovation Strategy (RIS) through the National Research Foundation of Korea (NRF) funded by the Ministry of Education (MOE) under Grant 2021RIS-003.

ABSTRACT This paper proposes a finite-time output controller to realize the tracking control of n degrees of freedom (n-DOF) manipulator, which can address the time-varying output constraints and uncertainties, such as modeling error, unknown frictions, and external disturbance. A nonlinear mapping is conducted to convert the constrained manipulator dynamics into unconstrained dynamics. Based on the unconstrained dynamics, a finite-time output controller is established based on the output-feedback control scheme and nonlinear extended state observer (NESO). Fractional order terms are exploited to obtain finite-time convergence, and the switching law is developed for the NESO to estimate both the unmeasured states and uncertainties. The superiority of the NESO and the stability of the overall system are theoretically demonstrated by using the Lyapunov approach. The effectiveness of the proposed controller is illustrated by conducting simulations and experiments with robot manipulators and comparing the obtained results with those of the existing techniques.

INDEX TERMS Robotic manipulator, output-feedback control, nonlinear extended state observer, nonlinear mapping, Lyapunov approach, time-varying output constraint.

I. INTRODUCTION

In modern industry, the physical interaction of humans and robotic systems is a critical aspect in robotic applications such as the rehabilitation of humans [1], exoskeletons [2], and cooperative manipulations [3]. Consequently, robotic manipulators are subject to strict regulations involving physical output constraints to ensure safe operation. These constraints partly originate from the intrinsic system specifications and state variables corresponding to the dead zone, hysteresis, saturation, and output performance [4]. Furthermore, the robotic outputs are critically regulated in predefined time-varying boundaries depending on the requirements of the applications, environmental information, or physical limitations [5]. Any violation of the constraints may lead to control performance degradation, system instability, and even system malfunction [6]. Recently, in the robot controller design, ensuring the system output performance while addressing the issues causing the transgression of the constraints has attracted considerable research attention.

To overcome the output constraints, the barrier Lyapunov function (BLF) [7] and the transformation technique [8] have been employed. The BLF was first proposed to address the *constant* output constraint issue in a nonlinear system [7]. Later, the *time-varying output constraints* were managed using the BLF [9]. In addition, the BLF has been used in combinations with some superior methods, such as fuzzy logic systems (FLSs) [10], and neural networks (NNs) [11], [12]

The associate editor coordinating the review of this manuscript and approving it for publication was Bidyadhar Subudhi.

to guarantee that the control requirements are obtained under the presence of the uncertainties and output constraints. It is difficult to apply this method for designing advanced controllers with finite time convergence expectation because of the complication in the BLF. A transformation method based on prescribed performance control was proposed [13]. The main idea is to convert the constrained system into an unconstrained one through the transformation of the output constrained errors. The output constrained functions were defined based on the transient and steady state of the output errors. Additionally, the transformed system owns the potential properties for developing advanced controllers to achieve the finite-time convergent goal. This technique has been conducted in many nonlinear systems, such as a flexible beam system [14], a single-link flexible joint robotic manipulator [15], a half-car active suspension system [16], and a small nonlinear UAV system [17]. Like the BLF, this method was also used in combinations with approximation structures, such as the FLS [18] and NN [19], to increase the position precision in the nonlinear system and avoid the contravention of the output constraints. Zhou et al. [20] developed an adaptive fuzzy backstepping control based on the transformation technique, which included the fuzzy approximator and backstepping technique, to control a non-strict feedback stochastic nonlinear system with uncertainties and output constraints. Moreover, an adaptive neural control was presented for an n-link robot manipulator subjected to uncertainties and output constraints [21]. The advanced control was realized based on an NN approximator and transformation technique.

Nevertheless, the NN and FLS implementation requires the practitioners to have considerable knowledge to select the parameters [22], such as the number of layers, number of nodes in a layer, learning rates, and initial weighting vector in the NN, or membership functions and fuzzy laws in the FLS, and intensive computations must be performed [23]. Therefore, this implementation is highly challenging. Notably, the extended state observer (ESO), proposed by Han [24], can be used to estimate both the unmeasured state and lumped uncertainties in nonlinear systems [25], in which the estimated errors converge in an infinite time. Lately, several nonlinear ESOs [26] have been investigated to enhance the estimation results and speed responses. In Yang et al. [27] developed the linear ESO to estimate the nonlinearities and unmeasured states of two flexible links manipulators. In Tran et al. [28] investigated a nonlinear ESO to estimate an unknown payload in a manipulator. The barrier Lyapunov function was used in the control design to manage the time-varying output constraints in the manipulator. In Nguyen et al. [29] derived a nonlinear ESO to handle the unknown uncertainties in the parallel manipulator. The nonsingular fast terminal sliding mode control guaranteed the finite convergence of the output tracking error in the controlled system. However, the aforementioned techniques [6], [7], [8], [9], [10], [11], [12], [13], [14], [15], [16], [17], [18], [19], [20], [21], [22] provide *asymptotical convergence in infinite time.* Considering these aspects, this paper proposes a solution that is easy to implement and can ensure *finite-time convergence*. The proposed solution guarantees that the output responses accomplish the time-varying output constraints with high accuracy and prompt convergence.

In particular, we first establish a finite-time output control to track the problem of an uncertain manipulator with time-varying output constraints. Then, the transforming technique is employed to convert the constrained dynamics system into an unconstrained one. Subsequently, a switching NESO is utilized to approximate a lumped uncertainty containing the modeling error, unknown friction, and external disturbance. This NESO is constructed by swapping a conventional linear ESO and a nonlinear ESO. The change event is specified by comparing the estimated error with the predefined positive value. This technique allows the NESO to yield enhanced estimation responses and avoid the singular issue. In the final step, the proposed control is developed using the transformed dynamics, switching NESO, and fractional auxiliaries in the control laws. The use of the auxiliaries helps increase the convergence rate of the output responses. Some simulation and experiment results were obtained by using 3 degrees of freedom (DOF) manipulator to exhibit the efficiency of the proposed control.

The main contributions of this work can be summarized as:

1) This paper first studies a finite-time output control for an n-DOF manipulator under the presence of modeling error, unknown frictions, external disturbance, and output constraint. The finite-time convergence of the output response in the manipulator is ensured by integrating the fraction order auxiliary in the full-state feedback control, which is designed from the transformed dynamics to overcome the time-varying output constraints. The stability, finite-time convergence, and constraint adherence of the proposed control over the n-DOF manipulator are theoretically analyzed by using the Lyapunov approach.

2) A switching NESO is used to estimate both the unmeasured states and lumped uncertainties in the n-DOF manipulator. Only the output feedback is required when using the estimated unmeasured states, and thus, the proposed control emerges as a finite-time output control scheme.

The remaining paper is constructed as follows. Section II describes the problem formulation and preliminaries. The NESO, finite-time full-state feedback control, and proposed control are elaborated in Section III. Section IV describes the numerical simulations conducted for a 3-DOF manipulator. Section V reports the experimental analysis conducted using a 3-DOF hydraulic manipulator test bench. Finally, Section VI presents some conclusions and future works.

II. PROBLEM DESCRIPTION AND PRELIMINARIES

A. PROBLEM DESCRIPTION

This study considers an n-DOF manipulator in the joint space whose dynamics can be presented as [30]

$$\mathbf{M}(\mathbf{q})\ddot{\mathbf{q}} + \mathbf{C}(\mathbf{q}, \dot{\mathbf{q}})\dot{\mathbf{q}} + \mathbf{G}(\mathbf{q}) + \mathbf{J}^T(\mathbf{q})\,\mathbf{f} + \boldsymbol{\tau}_{fric} = \boldsymbol{\tau} \quad (1)$$

where $\mathbf{q}, \dot{\mathbf{q}}, \ddot{\mathbf{q}} \in R^{n\times 1}$ represent the position, angular velocity, and angular acceleration vectors of each joint, respectively; $\mathbf{M}(\mathbf{q}) \in R^{n\times n}$ is the uniformly positive definite symmetric matrix of inertia; $\mathbf{C}(\mathbf{q}, \dot{\mathbf{q}}) \in R^{n\times n}$ presents the Coriolis and centrifugal term matrix; $\mathbf{G}(\mathbf{q}) \in R^{n\times 1}$ derives the gravity vector; τ is the torque acting on the joints; $\mathbf{J}(\mathbf{q})$ presents a nonsingular Jacobian matrix; $\boldsymbol{\tau}_{fric}$ represents the unknown frictions; and $\mathbf{f}$ represents the external disturbance.

In practice, it is difficult to determine the dynamics parameters of the robot. Thus, we define $(.) = (.)_0 + \Delta(.)$, where $(.)$ indicates $\mathbf{M}(\mathbf{q})$, $\mathbf{C}(\mathbf{q}, \dot{\mathbf{q}})$, or $\mathbf{G}(\mathbf{q})$; $(.)_0$ represents the nominal matrix or vector; and $\Delta(.)$ indicates the uncertainties.

Assumption 1: Assume that the unknown frictions and external disturbances are differentiable and bounded functions.

Property 1 [30]: $\dot{\mathbf{M}}(\mathbf{q}) - 2\mathbf{C}(\mathbf{q}, \dot{\mathbf{q}})$ is a skew-symmetric matrix, defined as $\mathbf{x}^T\left[\dot{\mathbf{M}}(\mathbf{q}) - 2\mathbf{C}(\mathbf{q}, \dot{\mathbf{q}})\right]\mathbf{x} = 0$.

Property 2 [31]: The inequality $\|G(q)\| \le \kappa_g$ is satisfied, where κ_g is a known positive constant.

Property 3 [31]: The inequality $\|C(q, \dot{q})\| \le \kappa_C \|\dot{q}\|$ holds where κ_C is a known positive constant.

Property 4 [31]: The inequality $m_1 \le \|\mathbf{M}(\mathbf{x}_1)\| \le m_2$ is satisfied where $m_i\,(i = 1, 2)$ are the positive constants.

Let $\mathbf{x}_1 = \mathbf{q} \in R^n$, and $\mathbf{x}_2 \in \dot{\mathbf{q}} \in R^n$. The robotic dynamics (1) can be described in the state space form as

$$\begin{aligned}\dot{\mathbf{x}}_1 &= \mathbf{x}_2\\ \dot{\mathbf{x}}_2 &= \mathbf{M}_0^{-1}(\mathbf{x}_1)\left(\mathbf{u} - \mathbf{C}_0(\mathbf{x}_1, \mathbf{x}_2)\mathbf{x}_2 - \mathbf{G}_0(\mathbf{x}_1) - \boldsymbol{\Delta}(t)\right)\end{aligned} \tag{2}$$

where $\mathbf{x}_i = [x_{i1}, x_{i2}, \ldots, x_{in}]^T, (i = 1, 2)$; and $\boldsymbol{\Delta}(t) = \Delta\mathbf{M}(\mathbf{x}_1)\dot{\mathbf{x}}_2 + \Delta\mathbf{C}(\mathbf{x}_1, \mathbf{x}_2)\mathbf{x}_2 + \Delta\mathbf{G}(\mathbf{x}_1) + \mathbf{J}^T(\mathbf{x}_1)\mathbf{f} + \boldsymbol{\tau}_{fric}$ presents a lumped disturbance, which consists of the modeling error, unknown friction, and external disturbance. $\mathbf{u}$ corresponds to the input torque $\boldsymbol{\tau}$.

The control goal is to track a reference $\mathbf{x}_d = [x_{d1}, x_{d2}, \ldots, x_{dn}]^T$ while guaranteeing the satisfaction of the system output constraints $\underline{x_{1i}}(t) < x_{1i}(t) < \overline{x_{1i}}(t)$, where $\underline{\mathbf{x}_1}(t) = \left[\underline{x_{11}}(t), \ldots, \underline{x_{1n}}(t)\right]^T$ and $\overline{\mathbf{x}_1}(t) = \left[\overline{x_{11}}(t), \ldots, \overline{x_{1n}}(t)\right]^T$ express lower boundary and upper boundary function vector.

Assumption 2: The trajectory signals $x_{di}, i = 1, 2, \ldots, n$ are assumed to be bounded and known, satisfying $|x_{di}| \le \bar{X}_{di}$, where $\bar{X}_{di}$ is a positive constant.

B. PRELIMINARIES

Notation 1:

$$y^c = |y|^c \, sign(y), \quad where\ c > 0 \tag{3}$$

It can be computed that

$$\frac{d}{dt}y^c = c\,|y|^{c-1}\,\dot{y} \tag{4}$$

The power of the vector is defined as follows

$$\begin{aligned}\mathbf{y}^c &= \left[y_1^c, \ldots, y_n^c\right]^T \in R^n\\ |\mathbf{y}|^c &= diag\left(\left[y_1^c, \ldots, y_n^c\right]\right) \in R^{n\times n}\end{aligned} \tag{5}$$

Nonlinear Transformation: The tracking error vectors in the state space system (2) are defined as follows:

$$\mathbf{e}_1 = \mathbf{x}_1 - \mathbf{x}_d \tag{6}$$

This error is bounded by the lower and upper boundaries:

$$\underline{e_{1i}}(t) < e_{1i}(t) < \overline{e_{1i}}(t) \tag{7}$$

where $\underline{e_{1i}}(t)$ and $\overline{e_{1i}}(t)$ are the lower and upper boundaries of the error constraints, respectively, which are stated as follows:

$$\begin{aligned}\overline{e_{1i}}(t) &= \overline{x_{1i}}(t) - x_{di}(t) > 0\\ \underline{e_{1i}}(t) &= \underline{x_{1i}}(t) - x_{di}(t) < 0\end{aligned} \tag{8}$$

where $\overline{x_{1i}}(t)$ and $\underline{x_{1i}}(t)$ are the upper and lower boundaries of the output constraints, respectively.

To combine the errors $e_{1i}(t)$ with the constraints, a nonlinear transformation technique is adopted to incorporate the constrained tracking error in the system dynamics. The transformation equation [9] can be expressed as follows:

$$e_{1i}(t) = \overline{e_{1i}}(t)\,T_i(z_i(t), \eta_i(t)) \tag{9}$$

where $\eta_i(t) = \underline{e_{1i}}(t)\big/\overline{e_{1i}}(t)$, z_i is the new error variable, and $T_i(.)$ is an invertible and increasing function with respect to $z_i(t)$, which fulfills the bellow conditions:

$$\begin{aligned}\lim_{z_i(t)\to-\infty}(T_i(z_i(t), \eta_i(t))) &= \eta_i(t)\\ \lim_{z_i(t)\to+\infty}(T_i(z_i(t), \eta_i(t))) &= 1\end{aligned} \tag{10}$$

The new error variable, $z_i(t)$, can be rewritten as

$$z_i(t) = T_i^{-1}\left(\frac{e_{1i}(t)}{\overline{e_{1i}}(t)}, \eta_i(t)\right) \tag{11}$$

The following inequality holds:

$$\eta_i(t) < T_i(z_i(t), \eta_i(t)) < 1 \tag{12}$$

when the new variable $z_i(t)$ is bounded.

By substituting (8) and (9) into (12), we can derive the inequality as follows:

$$\underline{e_{1i}}(t) < \overline{e_{1i}}(t)\,T_i(z_i(t), \eta_i(t)) = e_{1i}(t) < \overline{e_{1i}}(t) \tag{13}$$

which indicates that the output responses are bounded by the time-varying output constraints, as presented in (7). In other words, the new variable $z_i(t)$ can be used to derive an unconstrained model from the constrained one with the error variable e_{1i}. $z_i(t)$ can be differentiated with time as follows:

$$\begin{aligned}\dot{z}_i = &\frac{\partial T_i^{-1}}{\partial\left(\frac{e_{1i}(t)}{\overline{e_{1i}}(t)}\right)}\frac{1}{\overline{e_{1i}}(t)}\left(\dot{e}_{1i}(t) - \frac{e_{1i}(t)\,\dot{\overline{e_{1i}}}(t)}{\overline{e_{1i}}(t)}\right)\\ &+ \frac{\partial T_i^{-1}}{\partial\eta_i(t)}\dot{\eta}_i(t)\end{aligned} \tag{14}$$

This expression is substituted in the first equation of (2) to achieve the unconstrained manipulator dynamics for the control design in the subsequent procedure.

III. CONTROL DESIGN

In this study, the lumped uncertainty $\mathbf{M}_0^{-1}(\mathbf{x}_1)\,\boldsymbol{\Delta}(t)$, of the manipulator dynamics (2) are considered and expanded to a state expressed as $\mathbf{x}_3 \in R^{n\times 1}$. The state variable is then described as $\mathbf{x} = \left[\mathbf{x}_1^T, \mathbf{x}_2^T, \mathbf{x}_3^T\right]^T \in R^{3n\times 1}$. In order to design and analyze the NESO, the manipulator dynamics (2) is rewritten as follows [32]:

$$\begin{aligned}\dot{\mathbf{x}}_1 &= \mathbf{x}_2\\ \dot{\mathbf{x}}_2 &= \mathbf{F}(\mathbf{x}_1, \mathbf{x}_2) + \mathbf{H}(\mathbf{x}_1)\,\mathbf{u} + \mathbf{x}_3\\ \dot{\mathbf{x}}_3 &= \boldsymbol{\delta}(t)\end{aligned} \tag{15}$$

where $\mathbf{x}_3 = -\mathbf{M}_0^{-1}(\mathbf{x}_1)\,\boldsymbol{\Delta}(t)$; $\boldsymbol{\delta}(t)$ is the differential state of $\dot{\mathbf{x}}_3$; $\mathbf{F}(\mathbf{x}_1, \mathbf{x}_2) = \mathbf{M}_0^{-1}(\mathbf{x}_1)\left(\mathbf{C}_0(\mathbf{x}_1, \mathbf{x}_2)\,\mathbf{x}_2 + \mathbf{G}_0(x_1)\right)$; and $\mathbf{H}(\mathbf{x}_1) = \mathbf{M}_0^{-1}(\mathbf{x}_1)$.

Assumption 3 [33]: According to *Assumption* 1, *Property 2*, *Property 3, Property 4*, and equation (11) in [34], the lumped uncertainties of the system are bounded by the function, $\|x_3\| \le b_0 + b_1\|x_1\| + b_2\|x_2\|^2$ with b_i $(i = 0, 1, 2)$ are constants. Because of the limited bandwidth of actuators in practice, the differentiation of the state $\mathbf{x}_3$ is supposed to be bounded, i.e., $\|\boldsymbol{\delta}(t)\|_\infty \le \overline{\delta}$, where $\overline{\delta}$ presents a positive constant.

Assumption 4: The functions $\mathbf{F}(\mathbf{x}_1, \mathbf{x}_2)$ are assumed as a local Lipschitz function with respect to $\mathbf{x}_2$ in the practical range.

A. NONLINEAR EXTENDED STATE OBSERVER

The NESO technique is adopted to address the unmeasured state vector $\mathbf{x}_2$ and estimate the lumped disturbance $\mathbf{x}_3$, thereby enhancing the real-time controller performance. To this end, the manipulator dynamics (11) are represented as

$$\begin{aligned}\dot{\mathbf{x}} &= \mathbf{A}_n\mathbf{x} + \mathbf{B}_n\mathbf{u} + \boldsymbol{\varphi}(\mathbf{x}) + \mathbf{D}(\mathbf{x})\\ \mathbf{y} &= \mathbf{x}_1\end{aligned} \tag{16}$$

where $\mathbf{A}_n = \begin{bmatrix}\mathbf{0}_{n\times n} & \mathbf{I}_{n\times n} & \mathbf{0}_{n\times n}\\ \mathbf{0}_{n\times n} & \mathbf{0}_{n\times n} & \mathbf{I}_{n\times n}\\ \mathbf{0}_{n\times n} & \mathbf{0}_{n\times n} & \mathbf{0}_{n\times n}\end{bmatrix} \in R^{3n\times 3n}$; $\mathbf{B}_n = \begin{bmatrix}\mathbf{0}_{n\times n}\\ \mathbf{H}(\mathbf{x}_1)\\ \mathbf{0}_{n\times n}\end{bmatrix} \in R^{3n\times n}$; $\boldsymbol{\varphi}(\mathbf{x}) = \begin{bmatrix}\mathbf{0}_{n\times 1}\\ \mathbf{F}(\mathbf{x})\\ \mathbf{0}_{n\times 1}\end{bmatrix} \in R^{3n\times 1}$; $\mathbf{D}(\mathbf{x}) = \begin{bmatrix}\mathbf{0}_{n\times 1}\\ \mathbf{0}_{n\times 1}\\ \boldsymbol{\delta}(t)\end{bmatrix} \in R^{3n\times 1}$; and $\mathbf{I}_{n\times n}$ and $\mathbf{0}_{n\times n}$ represent a unit matrix and zero matrices sized $n \times n$, respectively.

The following NESO is implemented,

$$\dot{\hat{\mathbf{x}}} = \mathbf{A}_n\hat{\mathbf{x}} + \mathbf{B}_n\mathbf{u} + \boldsymbol{\varphi}(\hat{\mathbf{x}}) + \boldsymbol{\Gamma}\mathbf{G}_{fal}(\tilde{\mathbf{x}}_1, \lambda) \tag{17}$$

where $\hat{\mathbf{x}}$ is derived from the estimated system state of $\mathbf{x}$, $\tilde{\mathbf{x}}$ shows the estimation error, derived as $\tilde{\mathbf{x}} = \mathbf{x} - \hat{\mathbf{x}}$, $\boldsymbol{\varphi}(\hat{\mathbf{x}}) = \left[\mathbf{0}_{n\times n}\ \mathbf{F}(\mathbf{x}_1, \hat{\mathbf{x}}_2)\ \mathbf{0}_{n\times n}\right]^T$, $\boldsymbol{\Gamma} = \left[3\gamma\mathbf{I}_{n\times n}\ 3\gamma^2\mathbf{I}_{n\times n}\ \gamma^3\mathbf{I}_{n\times n}\right]^T \in R^{3n\times n}$ is the observer gain matrix; $\gamma > 0$ is adapted to enhance the observer performances; $\mathbf{G}_{fal}(\tilde{\mathbf{x}}_1, \lambda) = \left[g_{fal}(\tilde{x}_{11}, \lambda)\ \ldots\ g_{fal}(\tilde{x}_{1n}, \lambda)\right]^T \in R^{n\times 1}$;

Remark 1: The switching observer vector, $G_{fal}(\tilde{x}_1, \lambda)$, in the NESO is used to enhance the estimation performance and avoid the singular issue.

The nonlinear function, $g_{fal}(\tilde{x}_{1i}, \lambda, \varepsilon)$, can be defined as

$$g_{fal}(\tilde{x}_{1i}, \lambda) = \begin{cases}0.5\left(\tilde{x}_{1i} + (\tilde{x}_{1i})^{\lambda}\right) & \|\tilde{x}_{1i}\|_2 > \varepsilon_{\tilde{x}}\\ \tilde{x}_{1i} & otherwise\end{cases} \tag{18}$$

where $\lambda = {}^{\lambda_1}\!/_{\lambda_2}$ is a positive constant; $0 < \lambda_1 < \lambda_2$ are odd constants; and $\varepsilon_{\tilde{x}}$ is a positive constant.

From (16) and (17), the state estimation error dynamics can be obtained as follows:

$$\dot{\tilde{\mathbf{x}}} = \mathbf{A}_n\tilde{\mathbf{x}} + \tilde{\boldsymbol{\varphi}}(\mathbf{x}) - \Gamma\mathbf{G}_{fal}(\tilde{\mathbf{x}}_1, \lambda) + \mathbf{D}(\mathbf{x}) \tag{19}$$

where $\tilde{\boldsymbol{\varphi}} \triangleq \boldsymbol{\varphi}(\mathbf{x}) - \boldsymbol{\varphi}(\hat{\mathbf{x}})$.

Based on *Assumption* 4, the following inequality holds with a known positive constant c.

$$|\tilde{\boldsymbol{\varphi}}| = \left|\boldsymbol{\varphi}(\mathbf{x}_2) - \boldsymbol{\varphi}(\hat{\mathbf{x}}_2)\right| \le c\,|\boldsymbol{\sigma}| \tag{20}$$

If $\boldsymbol{\sigma}_1 = \mathbf{G}_{fal}(\tilde{\mathbf{x}}_1, \lambda) \in R^{n\times 1}$, $\boldsymbol{\sigma}_i = \frac{\tilde{\mathbf{x}}_i}{\gamma^{i-1}} \in R^{n\times 1}$ $(i = 2, 3)$, the corresponding derivatives with respect to time are presented as

$$\begin{aligned}\dot{\boldsymbol{\sigma}}_1 &= diag(\boldsymbol{\mu})\,\dot{\mathbf{x}}_1 = \gamma\, diag(\boldsymbol{\mu})\,\boldsymbol{\sigma}_2 - 3\gamma\, diag(\boldsymbol{\mu})\,\boldsymbol{\sigma}_1\\ \dot{\boldsymbol{\sigma}}_2 &= \frac{1}{\gamma}\dot{\tilde{\mathbf{x}}}_2 = \gamma\sigma_3 + \frac{\tilde{F}(\mathbf{x}_1, \mathbf{x}_2)}{\gamma} - 3\gamma\boldsymbol{\sigma}_1\\ \dot{\boldsymbol{\sigma}}_3 &= \frac{1}{\gamma^2}\dot{\tilde{\mathbf{x}}}_3 = \frac{\boldsymbol{\delta}(t)}{\gamma^2} - \gamma\boldsymbol{\sigma}_1\end{aligned} \tag{21}$$

where $\boldsymbol{\mu} = [\mu_1, \ldots, \mu_n]^T = \left[\frac{\partial g_{fal}(\tilde{x}_{11}, \lambda)}{\partial \tilde{x}_{11}}, \ldots, \frac{\partial g_{fal}(\tilde{x}_{1n}, \lambda)}{\partial \tilde{x}_{1n}}\right]$.

Furthermore, the NESO (19) is rewritten as follows:

$$\dot{\boldsymbol{\sigma}} = \gamma\mathbf{A}_{n1}\boldsymbol{\sigma} + \frac{\tilde{\boldsymbol{\varphi}}}{\gamma} + \frac{\mathbf{D}(\mathbf{x})}{\gamma^2} \tag{22}$$

where $\mathbf{A}_{n1} = \begin{bmatrix}-3diag(\boldsymbol{\mu}) & diag(\boldsymbol{\mu}) & \mathbf{0}_{n\times n}\\ -3\mathbf{I}_{n\times n} & \mathbf{0}_{n\times n} & \mathbf{I}_{n\times n}\\ -\mathbf{I}_{n\times n} & \mathbf{0}_{n\times n} & \mathbf{0}_{n\times n}\end{bmatrix} \in R^{3n\times 3n}$ is a negative definite matrix.

In the first condition, $\|\tilde{x}_{1i}\|_2 > \varepsilon_{\tilde{x}}$, the differential $g_{\mathbf{fal}}$ function (18) with respect to time can be computed as follows:

$$\dot{g}_{fal}(\tilde{x}_{1i}, \lambda) = 0.5\dot{\tilde{x}}_{1i}\left(1 + \lambda\,|\tilde{x}_{1i}|^{\lambda-1}\right) = \mu_i\dot{\tilde{x}}_{1i} \tag{23}$$

where $\mu_i = 0.5\left(1 + \lambda\,|\tilde{x}_{1i}|^{\lambda-1}\right)$ $(i = 1, \ldots, n)$ are positive bounded functions.

Remark 2: The $\varepsilon_{\tilde{x}}$ is selected how the μ_i is positive functions and the matrix $\mathbf{A}_{n1}$ is a negative definite matrix.

In the second condition, $\|\tilde{x}_{1i}\|_2 \le \varepsilon_{\tilde{x}}$,the differential g_{fal} function (18) with respect to time is represented as follows: $\dot{g}_{fal}(\tilde{x}_{1i}, \lambda) = \dot{\tilde{x}}_{1i}$ and $\mu_i = 1$.

Theorem 1: When the inequality (20) and *Assumption* 2 hold in the switching NESO (17), the estimation errors are

expected to reach and remain in a predefined region with finite time by a suitable constant γ.

This theorem is proven and expressed in **Appendix A**.

B. FINITE FULL STATE FEEDBACK CONTROL WITH THE TIME-VARYING OUTPUT CONSTRAINT

According to Section II. B, the manipulator dynamics with the output constraint in (2) can be transformed to the following unconstrained system:

$$\begin{aligned}\dot{\mathbf{z}}_1 &= \mathbf{\Phi}\mathbf{x}_2 + \mathbf{\Psi} \\ \dot{\mathbf{x}}_2 &= \mathbf{M}_0^{-1}(\mathbf{x}_1)\left(\mathbf{u} - \mathbf{C}_0(\mathbf{x}_1, \mathbf{x}_2)\mathbf{x}_2 - \mathbf{G}_0(\mathbf{x}_1) - \Delta\right)\end{aligned} \tag{24}$$

where

$$\mathbf{\Phi} = \begin{bmatrix} \dfrac{\partial T_1^{-1}}{\partial\left(\dfrac{e_{11}}{\overline{e_{11}}}\right)}\dfrac{1}{\overline{e_{11}}} & \cdots & 0 \\ \vdots & \ddots & \vdots \\ 0 & \cdots & \dfrac{\partial T_n^{-1}}{\partial\left(\dfrac{e_{1n}}{\overline{e_{1n}}}\right)}\dfrac{1}{\overline{e_{1n}}} \end{bmatrix} \in R^{n\times n} \tag{25}$$

$$\begin{aligned}\mathbf{\Psi} = -\mathbf{H}\dot{\mathbf{x}}_d - &\begin{bmatrix} \dfrac{\partial T_1^{-1}}{\partial\left(\dfrac{e_{11}(t)}{\overline{e_{11}}(t)}\right)}\dfrac{1}{\overline{e_{11}}(t)}\dfrac{e_{11}(t)\dot{\overline{e_{11}}}(t)}{\overline{e_{11}}(t)} \\ \vdots \\ \dfrac{\partial T_n^{-1}}{\partial\left(\dfrac{e_{1n}(t)}{\overline{e_{1n}}(t)}\right)}\dfrac{1}{\overline{e_{1n}}(t)}\dfrac{e_{1n}(t)\dot{\overline{e_{1n}}}(t)}{\overline{e_{1n}}(t)} \end{bmatrix} \\ &+ \begin{bmatrix} \dfrac{\partial T_1^{-1}}{\partial(\eta_1(t))}\dot{\eta}_1(t) \\ \vdots \\ \dfrac{\partial T_2^{-1}}{\partial(\eta_2(t))}\dot{\eta}_2(t) \end{bmatrix}\end{aligned} \tag{26}$$

$$T_i(z_i(t), \eta_i(t)) = \frac{e^{z_i(t)} + \eta_i(t)\, e^{-z_1(t)}}{e^{z_i(t)} + e^{-z_1(t)}} \tag{27}$$

Remark 3: In this case study, we assume that all state variables in the manipulator consist of position and velocity variables are measured by the respective sensors.

The tracking errors in the system (24) are presented as the following:

$$\mathbf{e}_z = \mathbf{z}_1; \quad \mathbf{e}_2 = \mathbf{x}_2 - \boldsymbol{\alpha}_1 \in R^{n\times 1} \tag{28}$$

where $\boldsymbol{\alpha}_1$ is the virtual control vector.

This virtual control is selected to be:

$$\boldsymbol{\alpha}_1 = \mathbf{\Phi}^{-1}\left(-\mathbf{K}_{10}\mathbf{e}_z - \mathbf{K}_{11}\mathbf{e}_z^{\beta_2} - \mathbf{\Psi}\right) \tag{29}$$

where $\mathbf{K}_{1i} \in R^{n\times n}\ (i = 0, 1)$ are positive diagonal matrices; and $0 < \beta_2 < 1$ is a positive constant.

The control law of the finite full-state feedback control with the time-varying output constraint is presented as follows:

$$\begin{aligned}\mathbf{u} = &-\mathbf{\Phi}\mathbf{e}_z - \mathbf{K}_{20}\mathbf{e}_2 - \mathbf{K}_{21}\mathbf{e}_2^{\beta_2} + \mathbf{C}_0(\mathbf{x}_1, \mathbf{x}_2)\boldsymbol{\alpha}_1 + \mathbf{G}_0(\mathbf{x}_1) \\ &+ \mathbf{M}_0(\mathbf{x}_1)\dot{\boldsymbol{\alpha}}_1\end{aligned} \tag{30}$$

where $\mathbf{K}_{2i} \in R^{n\times n}\ (i = 0, 1)$ presents a positive diagonal matrix.

Theorem 2: When control laws (29) and (30) are conducted for the manipulator whose dynamics is presented in (24), they will guarantee the finite-time stability and the output constraint satisfaction for the manipulator. The residual set of the manipulator is derived as follows:

$$\lim_{t-T_r} V(e) \le \min\left\{\frac{\delta_0}{(1-\varphi_0)\kappa_1}, \left(\frac{\delta_0}{(1-\varphi_0)\kappa_2}\right)^{\frac{2}{1+\beta_2}}\right\} \tag{31}$$

where $0 < \varphi_0 < 1; \kappa_2 = \min(\lambda_{\min}(\mathbf{K}_{11}), \lambda_{\min}(\mathbf{K}_{21}\mathbf{M}^{-\frac{1+\beta_2}{2}}))$; $\kappa_1 = \min(\lambda_{\min}(\mathbf{K}_{10}), \lambda_{\min}((\mathbf{K}_{20} - \Delta\mathbf{C}(\mathbf{x}_1, \mathbf{x}_2) - \frac{1}{2}\mathbf{I}_{n\times n})\mathbf{M}^{-1}))$; $\delta_0 = \frac{1}{2}\max(\mathbf{\Delta}^T(t)\mathbf{\Delta}(t) + \dot{\boldsymbol{\alpha}}_1^T\Delta\mathbf{M}^T\Delta\mathbf{M}\dot{\boldsymbol{\alpha}}_1)$; and $\mathbf{e} = \left[\mathbf{e}_z^T\ \mathbf{e}_2^T\right]^T$. The finite time is

$$T_r \le \max\left\{\begin{aligned} &t_0 + \frac{2}{\varphi_0(1-\beta_2)}\ln\frac{\varphi_0\kappa_1 V^{\frac{1+\beta_2}{2}}(e(t_0)) + \kappa_2}{\kappa_2}, \\ &t_0 + \frac{2}{\kappa_1(1-\beta_2)}\ln\frac{\kappa_1 V^{1-\beta_2}(e(t_0)) + \varphi_0\kappa_2}{\varphi_0\kappa_2}\end{aligned}\right\} \tag{32}$$

Theorem 2 is proven and described in **Appendix B**.

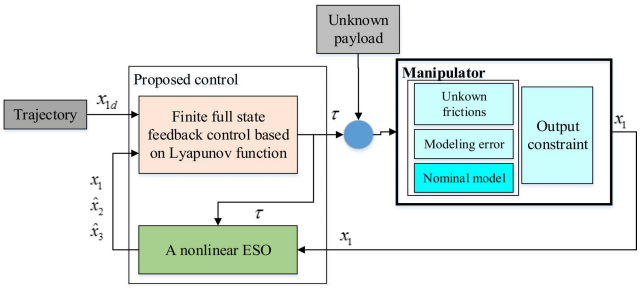

FIGURE 1. Schematic of the proposed control with the uncertain manipulator.

C. PROPOSED CONTROL

This Section describes the finite-time output controller. The proposed control consists of a finite full-state feedback control scheme and a switching NESO, as presented in FIGURE **1**. In this study, the proposed control must face the challenges of unknown payload, frictions, modeling error, and output constraints. Therefore, the observer estimates both the unmeasured states and lumped uncertainty. The finite full state feedback control is developed from the free constrained system dynamics to manage the varying time output

constraint and ensure the finite-time convergence of the output response, as shown in Section III-B. Consequently, the proposed control only requires the output angle and can be considered as a type of output feedback control.

Based on (29), (30), and (17), the proposed control law can be expressed as follows:

$$\boldsymbol{\alpha}_1 = \boldsymbol{\Phi}^{-1}\left(-\mathbf{K}_{10}\mathbf{e}_z - \mathbf{K}_{11}\mathbf{e}_z^{\boldsymbol{\beta}_2} - \boldsymbol{\Psi}\right) \tag{33}$$

$$\begin{aligned}\mathbf{u} = &-\boldsymbol{\Phi}\mathbf{e}_z - \mathbf{K}_{20}\hat{\mathbf{e}}_2 - \mathbf{K}_{21}\hat{\mathbf{e}}_2^{\boldsymbol{\beta}_2} + \mathbf{C}_0\left(\mathbf{x}_1, \hat{\mathbf{x}}_2\right)\boldsymbol{\alpha}_1 \\ &+ \mathbf{G}_0\left(\mathbf{x}_1\right) + \mathbf{M}_0\left(\mathbf{x}_1\right)\dot{\boldsymbol{\alpha}}_1 - \mathbf{M}_0\left(\mathbf{x}_1\right)\hat{\mathbf{x}}_3\end{aligned} \tag{34}$$

where $\hat{\mathbf{e}}_2 = \hat{\mathbf{x}}_2 - \boldsymbol{\alpha}_1 \in R^{n\times 1}$.

Theorem 3: When the proposed control laws (33), (34) and NESO (17) are implemented on an uncertain manipulator with time-varying output constraints, they will guarantee the uniformly ultimately bounded of the entire controlled system and the satisfaction of the time-varying constraints.

Theorem 3 is proven and presented in **Appendix C**.

IV. NUMERICAL SIMULATIONS

A. SIMULATION DESCRIPTION

To exhibit the advantages of the proposed control, several simulations are implemented on a 3-DOF manipulator whose structure is illustrated in FIGURE 2. The detailed dynamics [35] and parameters are presented as follows $l_1 = 0.1$, $l_2 = 0.5$, $l_3 = 0.2$, $m_i\,(i = 1, 2, 3) = 0.5$, and $g = 9.81$.

FIGURE 2. Schematic of the 3-DOF robotic manipulator.

The challenges associated with the manipulator control, such as the unknown friction, measurement noise, and external disturbance, are considered in the simulation. The unknown friction model is derived as $\boldsymbol{\tau}_{fric} = \mathbf{b}\mathbf{x}_2 + \mathbf{c}\tanh\left(\frac{\mathbf{x}_2}{\boldsymbol{\psi}}\right)$, where $\mathbf{b} = 5\mathbf{I}_{3\times 3}$ and $\mathbf{c} = 5\,\mathbf{I}_{3\times 3}$represent viscous and static diagonal matrices, respectively; $\boldsymbol{\psi} = 50\mathbf{I}_{3\times 1}$is a positive matrix. The measurement noise is a white noise with a power of 57×10^{-8} and a sampling time of 0.1 s. An external disturbance along the z-axis of the Cartesian coordinates is considered, with a value of 0 and 100 N in the first and last 15 s, respectively. It is assumed that loss-efficiency-fault arises in three actuators. The remained efficiency of the actuators is 80%.

The initial states of the robot manipulator are set as$\mathbf{x}_1\,(0) = \begin{bmatrix}0 & 22.9 & 28.6\end{bmatrix}$ (deg .), and $\mathbf{x}_2\,(0) = [0, 0, 0]^T$. The reference signal in the joint space is set as $\mathbf{x}_d = \left[45\sin\left(2\pi f_{fre}t\right), 22.5\sin\left(2\pi f_{fre}t + 0.5\right) + 30, 30\sin\left(2\pi f_{fre}t + 0.5\right) + 45\right]$ (deg .) where f_{fre} is the frequency of the reference.

Remark 4: Because of the physical limitations of the mechanical or electronic components in practice, the input controls of the manipulator are bounded. To ensure the simulation mimics a real test rig, the control signals of the controlled are limited as follows:

$$u = sat\,(u_{in}) = \begin{cases}\bar{u} & if\ u_{in} \geq \bar{u} \\ \underline{u} & if\ u_{in} \leq u \\ u_{in} & otherwise\end{cases} \tag{35}$$

where $\underline{u} = -2 \times 10^3 N.m$and $\bar{u} = 2 \times 10^3 N.m$ denote the minimum and maximum outputs, respectively.

B. SIMULATION RESULTS

To evaluate the superiority of the proposed control, we consider two other controllers: *the first controller* is a backstepping controller (BC) derived as $\boldsymbol{\alpha}_1 = \mathbf{x}_{2d} - \mathbf{K}_1\mathbf{e}_1$; $\mathbf{u}\,(t) = -\mathbf{K}_2\mathbf{e}_2 + \mathbf{C}_0\left(\mathbf{x}_1, \mathbf{x}_2\right)\boldsymbol{\alpha}_1\,(t) + \mathbf{G}_0\left(\mathbf{x}_1\right) + \mathbf{M}_0\left(\mathbf{x}_1\right)\dot{\boldsymbol{\alpha}}_1 - \mathbf{e}_1$, and *the second controller* pertains to the finite backstepping control based new state transformation (FBCST) expressed in (29) and (30). The working frequency is 0.5 Hz. The parameters of the controllers are selected as follows: **BC**$K_1 = 15diag\left([3, 5, 4]\right), K_2 = 75diag\left([1, 1, 1]\right)$; **FBCST** $\beta = 7/9$, $K_{10} = 5diag\left([3, 5, 4]\right)$; , $K_{11} = 10diag\left([3, 5, 4]\right)$, $K_{20} = 15diag\left([1, 1, 1]\right)$, $K_{21} = 60diag\left([1, 1, 1]\right)$; **Proposed controller** $K_{10} = 5diag\left([3, 5, 4]\right)$; , $K_{11} = 10diag\left([3, 5, 4]\right)$, $K_{20} = 15diag\left([1, 1, 1]\right)$, $K_{21} = 60diag\left([1, 1, 1]\right)$, $\beta = 7/9$, $e_1\,(t) = -\bar{e}_1\,(t)$, $\varepsilon_{\tilde{x}} = 2.8$, $\lambda = 0.91$, $\bar{e}_1\,(t) = \left(0.8e^{-0.4t} + 5.10^{-3}\right)\begin{bmatrix}1 & 1 & 1\end{bmatrix}^T\,(rad)$, $\kappa_0 = 180diag\left([1, 1, 1]\right)$. The controllers are implemented in MATLAB 2019a with an automatic solver and sampling time of 10^{-3} s.

Remark 5: To ensure a fair in comparison between the proposed control, FBCST, and BC, the FBCST parameters are extracted from the BC, and the proposed control parameters are inherited from the FBCST. These parameters are chosen by the trial-error method. The output constraints are provided based on the requirements for the initial and steady-state errors.

Remark 6: The controls are tuned considering the associated tradeoffs. The control gains K_{10} and K_{20} are selected to maintain the system stability. Additionally, the control gains K_{11} and K_{21} are selected to ensure the system stability and finite-time convergence of the output responses. Because of the physical restrictions in actuators, an excessively high K_{11} and K_{21} may lead to the chattering effect in the control signal, which may result in instability. Consequently, we implement the control gains K_{10} and K_{20} in control laws. Furthermore, β_2 is selected as a positive value smaller than 1.

FIGURE 3 describes the angular position responses in three joints of the manipulator with three controllers, with those of the BC, FBCST, and proposed control represented as a blue dashed line, a pink dot-dashed line, and a red line, respectively. The initial outputs of the manipulator with

the three controllers are set between the upper and lower boundaries, and the output responses track the references.

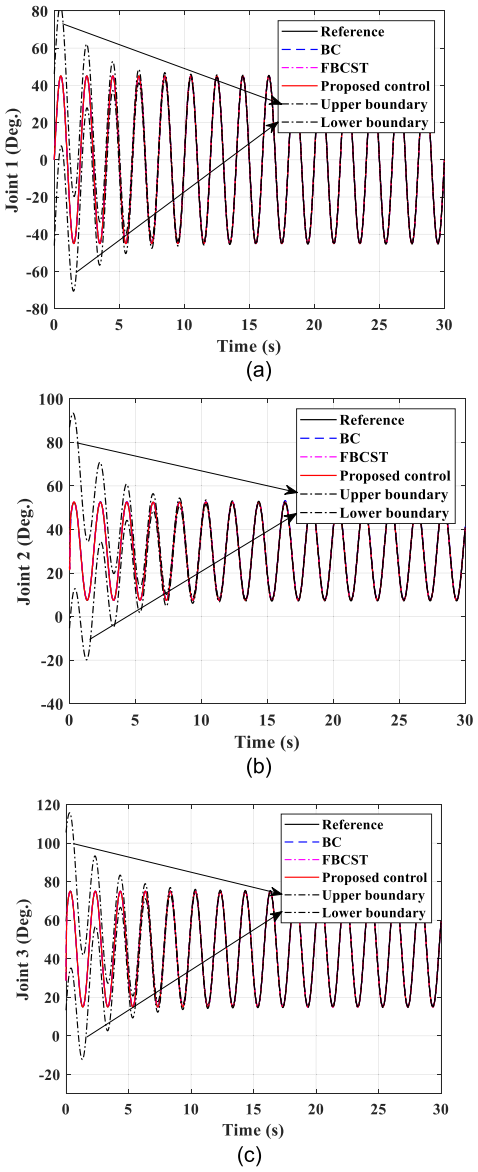

FIGURE 3. Output performance of the 3-DOF manipulator in three joints with reference at 0.5hz.

In addition, the errors between the output performances and references in FIGURE 4 indicate that the lumped uncertainty in the robotic manipulator causes significant errors in the case of BC (black line) in the first 15 s. Nevertheless, these errors belong to the predefined constraints, $\bar{e}_{1i}(t), e_{1i}(t), (i = 1, 2, 3)$ (black dashed-dot line), in this period. In the last 15 s, an external disturbance suddenly arises at the end-effector. Therefore, the errors exceed the predefined performances, as shown in FIGURE 4b and c. In the case of the FBCST (dot-dashed blue line) and proposed control (red line), the errors remain in the predefined constraints owing to the new state transformation, and the transient responses are faster than those of the BC due to

TABLE 1. RMS Tracking Error of Three Controllers in the joints (from 0.1 to 30 s).

Control methods	1st Joint	2nd Joint	3rd Joint
BC	9.2×10^{-2}	0.2142	6.39×10^{-2}
FBCST	7.1×10^{-3}	1.11×10^{-2}	3.8×10^{-3}
Proposed control	6×10^{-4}	4×10^{-4}	1.2×10^{-4}

the fractional terms in the controllers. The accuracy of the proposed control is higher than that of the FBCST because of the NESO utilization. The root mean square (RMS) values of the tracking errors of three controllers in the joints, as listed in TABLE 1, highlight the efficiency of the proposed control.

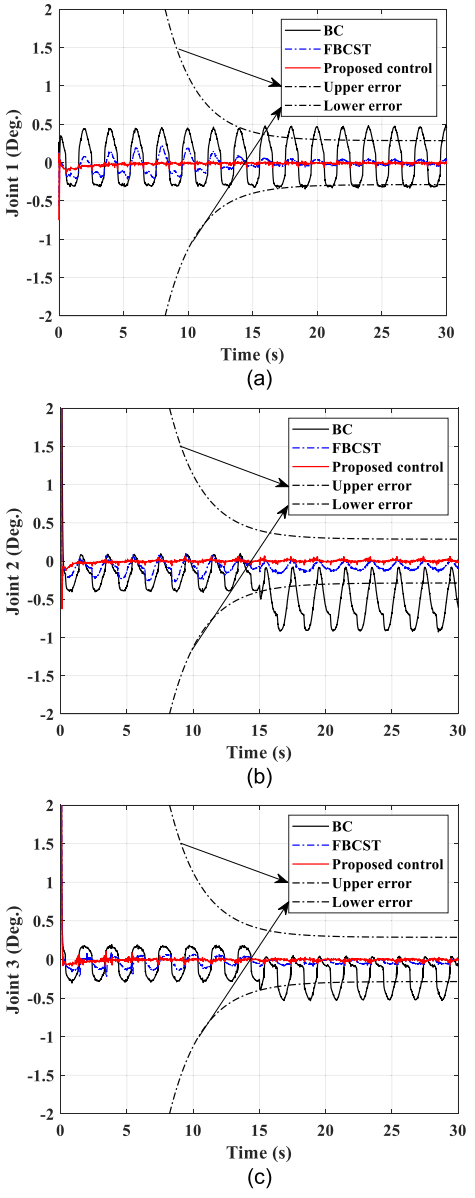

FIGURE 4. Tracking errors of the 3-DOF manipulator in three joints with reference at 0.5Hz.

FIGURE 5 presents the estimations of the unmeasured states in the 1st, 2nd, and 3rd joints of the manipulator, with the black and red lines indicating the unmeasured velocities and estimation results, respectively. The NESO successfully

estimates and reduces the measurement noises. The bandwidth of the NESO can be adjusted by selecting γ suitably. FIGURE 6 shows the estimated lumped disturbance responses of the NESO in the 1st, 2nd, and 3rd joints, represented as the blue dashed line, black dotted-dashed line, and red dashed line, respectively. In the first 15 s, the estimated disturbances are non-zero, although the external force has not emerged at the end-effector. These results are influenced by the presence of unknown frictions and measurement noise. In the last 15 s, an external force of 100 N is applied at the end-effector along the z-axis in the Cartesian coordinate. According to the geometric structure of the robotic manipulator, the external force impacts the 2nd and 3rd joints. Consequently, the estimated auxiliary variables in the 2nd and 3rd joints change considerably more than for the 1st Joint, as shown in FIGURE 6.

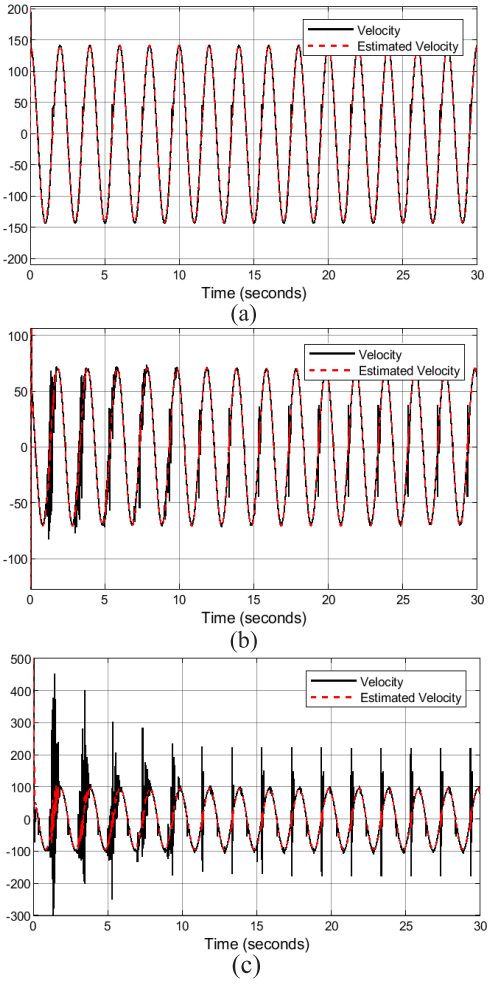

FIGURE 5. Estimated results of the velocity states in the NESO in three joints with references at 0.5 Hz.

In order to exhibit the effectiveness of the NESO, the estimated results in FIGURE 6 are converted into the estimated uncertainties in each joint and compared with the lumped ones, respectively. FIGURE 7 shows that the NESO well approximated the lumped uncertainties, including modeling

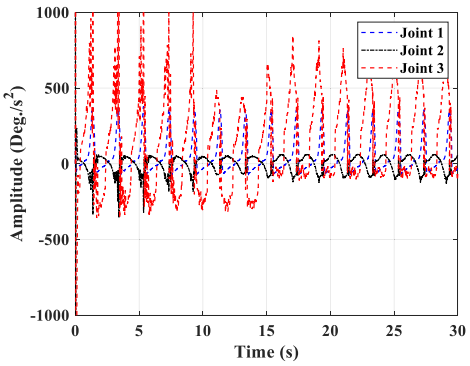

FIGURE 6. Estimated disturbance responses of the NESO in three joints with references at 0.5 Hz.

error, external disturbance, unknown frictions, and loss efficiency fault of three actuators.

V. EXPERIMENTAL STUDIES

A. EXPERIMENTAL DESCRIPTIONS

To further demonstrate the efficiency of the proposed control methodology, comparative experiments are conducted. The platform consists of a system analysis framework and a practical test bench, as presented in FIGURE 8. The test bench includes a hydraulic unit to supply power and the 3-DOF hydraulic manipulator. As mentioned previously, the hydraulic manipulator is constructed to have two rotary actuators to control the first and second joints. The third Joint is manipulated using a cylinder. Each joint is equipped with rotary incremental encoders (E40H6-5000-3-V-5) to measure real-time angle position. The practical testbench synchronously communicates with the system analysis through the Terminal 68LPR set up inside the control box and DAQ card (PCIe-6363) istalled in the PC. The control algorithms are implemented on MATLAB by using the real-time window target tool with a sample time of 10^{-3} s.

The desired trajectories for the hydraulic manipulator are chosen as $\mathbf{x}_d = [25\sin(\pi t), -20\cos(\pi t) + 30, 20\sin(\pi t) + 40]^T$ (deg.). The upper and lower boundaries are selected as $\bar{\mathbf{e}}_1(t) = \left(85e^{-0.9t} + 1.1\right)\left[1\ 1\ 1\right]^T$ (deg.), and $e_1(t) = -\bar{e}_1(t)$, respectively. The initial values are $\mathbf{x}_1(0) = \left[-55\ -17\ 3\right]^T$ (deg.) and $\mathbf{x}_2(0) = [0, 0, 0]^T$ (deg/s).

B. EXPERIMENTAL RESULTS

The experimental results of the proposed control are compared with those of the BC to prove the superiority of the proposed approach in satisfying the time-varying output constraints, compensating for the lumped disturbance, and enhancing the transient responses. The relationship between the output torque and input voltage in the hydraulic manipulator is a nonlinear function due to the nonlinear functions in the servo valves. In this study, we consider that this relationship is a linear function. In this case, the modeling error includes the actuator and manipulator dynamics, which pertain to the

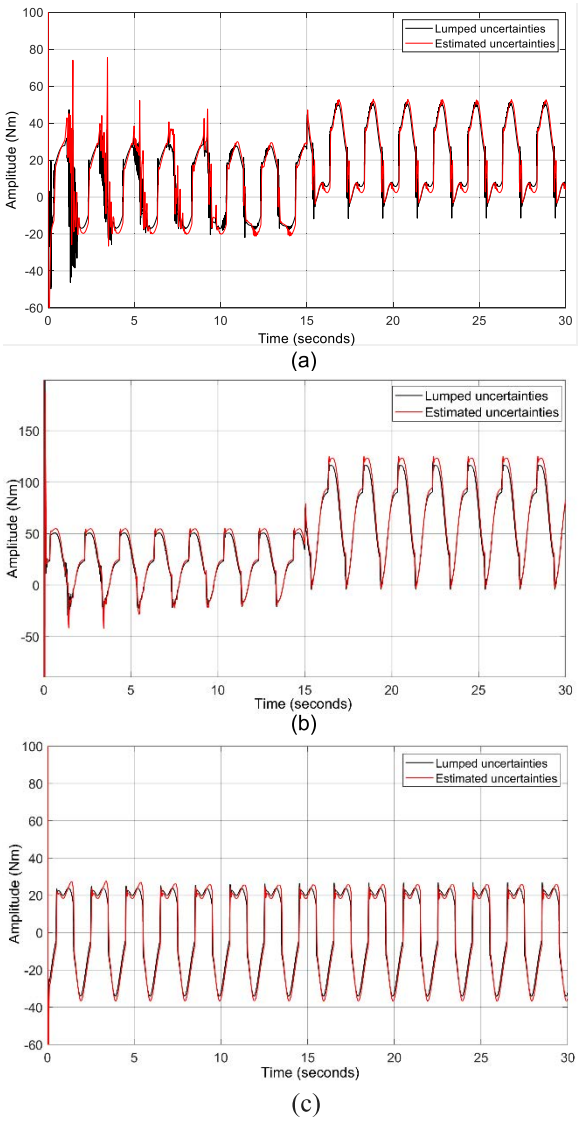

FIGURE 7. Comparison of the lumped uncertainties and the estimated ones in a) joint 1, b) joint 2, c) joint 3.

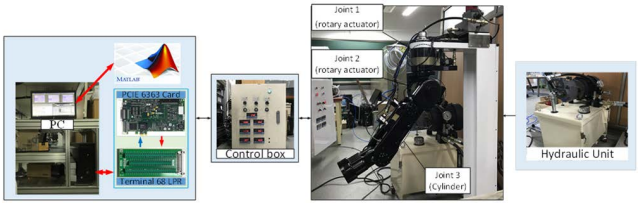

FIGURE 8. Experimental platform for the hydraulic manipulator.

identification methods. In the simulation section, the friction models are unknown functions, which are considered to be modeling errors. The parameters of the manipulator dynamics are the same as those specified in the simulation section.

The results presented in FIGURE 9. indicate that the error responses of the proposed control (red line) are bounded in the time-varying output constraints (dashed black line),

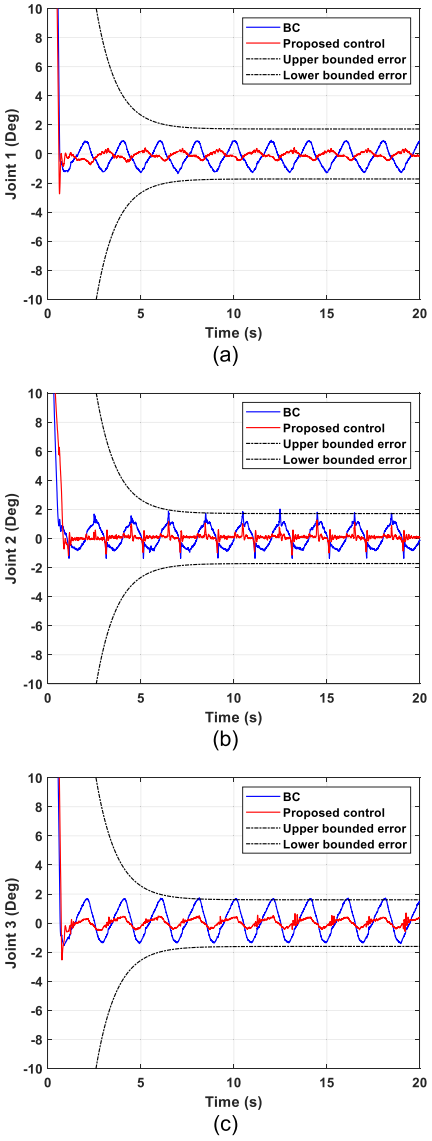

FIGURE 9. Tracking error responses of the BC and proposed control in three joints.

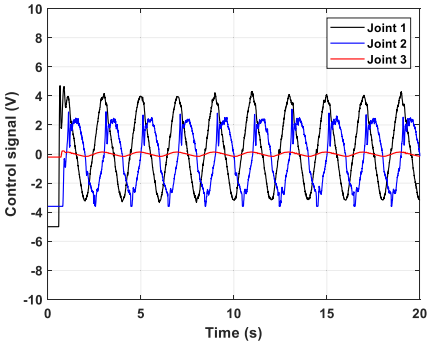

FIGURE 10. Control signals for the proposed control scheme.

with a steady-state value of 1.9°. The error responses of the BC (black line) do not satisfy the output constraints.

Additionally, the NESO in the proposed control estimated and compensated well for the lumped uncertainties in the real model. Consequently, the accuracy of the controlled system with the proposed control is better than the BC. The control signals, as electronic signals, are depicted in FIGURE 10. The experimental results validate the advantages of the proposed control.

VI. CONCLUSION AND FUTURE WORKS

This study proposed an advanced finite-time output control for uncertain robot manipulators with time-varying output constraints. A transformation technique was utilized to convert the constrained system into an unconstrained one to prevent the violation of the output constraint. A switching NESO, constructed by swapping the nonlinear ESO and traditional ESO, was utilized to estimate the unmeasured states and approximate the lumped uncertainty, including the unknown friction and external disturbance. The proposed control was developed by combining the transformed dynamics, switching NESO, and fractional auxiliaries in the control laws. The use of the auxiliaries ensured the finite-time convergence of the output responses. Then, the advantages of the proposed controller are satisfying the time-varying output constraints, achieving high accuracy, and prompt convergence. The stability and robustness of the proposed control are demonstrated based on the Lyapunov theory. The effectiveness of the proposed controller was demonstrated through both simulations and experiments.

For future work, the accuracy of the robotic manipulator can be improved when the advanced controller is developed according to the approach in [36]. The manipulator dynamics will be analyzed, including actuator dynamics, and the adaptive neural network will be used to approximate the modeling errors of the manipulator.

APPENDIX A

To demonstrate Theorem 1, we consider a Lyapunov function as follows:

$$V_0 = \frac{1}{2}\boldsymbol{\sigma}^T\mathbf{P}\boldsymbol{\sigma} \tag{36}$$

where $\boldsymbol{P}$ presents a positive definite matrix. The matrix, $\boldsymbol{P}$, is chosen to satisfy the below qualification

$$\mathbf{A}_{n1}^T\mathbf{P} + \mathbf{P}\mathbf{A}_{n1} = -2\mathbf{I}_{3n\times 3n} \tag{37}$$

From (22), the time derivative of the Lyapunov function (36) is depicted as

$$\begin{aligned}\dot{V}_0 &= \frac{1}{2}\gamma\boldsymbol{\sigma}^T\left(\mathbf{A}_{n1}^T\ \mathbf{P} + \mathbf{P}\mathbf{A}_{n1}\right)\boldsymbol{\sigma} + \frac{1}{2}\left(\frac{\tilde{\boldsymbol{\varphi}}}{\gamma} + \frac{\mathbf{D}(\mathbf{x})}{\gamma^2}\right)^T\mathbf{P}\boldsymbol{\sigma} \\ &\quad + \frac{1}{2}\boldsymbol{\sigma}^T\mathbf{P}\left(\frac{\tilde{\boldsymbol{\varphi}}}{\gamma} + \frac{\mathbf{D}(\mathbf{x})}{\gamma^2}\right) \\ &= -\gamma\boldsymbol{\sigma}^T\boldsymbol{\sigma} + \left(\frac{\tilde{\boldsymbol{\varphi}}}{\gamma} + \frac{\mathbf{D}(\mathbf{x})}{\gamma^2}\right)^T\mathbf{P}\boldsymbol{\sigma} \\ &\le \left(-\left(\gamma - \frac{c\lambda_{\max}(\mathbf{P})}{\gamma}\right)\|\boldsymbol{\sigma}\|_2 + \frac{\bar{\delta}}{\gamma^2}\lambda_{\max}(\mathbf{P})\right)\|\boldsymbol{\sigma}\|_2\end{aligned} \tag{38}$$

The differential Lyapunov function (38) with respect to time is a negative function when $-\left(\gamma - \frac{c\lambda_{\max}(\mathbf{P})}{\gamma}\right)\|\boldsymbol{\sigma}\|_2 + \frac{\bar{\delta}}{\gamma^2}\lambda_{\max}(\mathbf{P}) \le 0$ that means $\|\boldsymbol{\sigma}\|_2 \ge \frac{\bar{\delta}}{\gamma(\gamma^2 - c\lambda_{\max}(\mathbf{P}))}\lambda_{\max}(\mathbf{P})$. When the bandwidth γ is increased, the estimation errors in NESO are decreased, and the stability of the NESO is guaranteed [37].

APPENDIX B

In the first step, the virtual control is designed such that the new error approaches zero in a finite time. A candidate Lyapunov function is chosen as follows:

$$V_1 = \frac{1}{2}\mathbf{e}_z^T\mathbf{e}_z \tag{39}$$

By taking the time derivative of the Lyapunov function (39), and combining it with the first equation in (24). Its result is presented as follows:

$$\dot{V}_1 = \mathbf{e}_z^T\dot{\mathbf{e}}_z = \mathbf{e}_z^T\left(\boldsymbol{\Phi}\mathbf{x}_2(t) + \boldsymbol{\Psi}\right) \tag{40}$$

From (28) and (29), the equation (40) is represented as:

$$\begin{aligned}\dot{V}_1 &= \mathbf{e}_z^T\left(\boldsymbol{\Phi}(\mathbf{e}_2 + \boldsymbol{\alpha}_1) + \boldsymbol{\Psi}\right) \\ &= -\mathbf{e}_z^T\mathbf{K}_{10}\mathbf{e}_z - \mathbf{e}_z^T\mathbf{K}_{11}\mathbf{e}_z^{\beta_2} + \mathbf{e}_z^T\boldsymbol{\Phi}\mathbf{e}_2\end{aligned} \tag{41}$$

In the next step, the control law is constructed to guarantee that the velocity vector will approach zero in finite time. Now the Lyapunov function is selected as follows:

$$V_2 = V_1 + \frac{1}{2}\mathbf{e}_2^T\mathbf{M}\mathbf{e}_2 \tag{42}$$

Differentiating V_2 with respect to time shows as

$$\dot{V}_2 = \dot{V}_1 + \mathbf{e}_2^T\mathbf{M}\dot{\mathbf{e}}_2 + \frac{1}{2}\mathbf{e}_2^T\dot{\mathbf{M}}\mathbf{e}_2 \tag{43}$$

When we apply Property 1 to (43), its result yields

$$\dot{V}_2 = \dot{V}_1 + \mathbf{e}_2^T\left(\mathbf{M}(\mathbf{x}_1)\dot{\mathbf{e}}_2 + \mathbf{C}(\mathbf{x}_1, \mathbf{x}_2)\mathbf{e}_2\right) \tag{44}$$

Replacing (24), and (30) into (44), we get

$$\begin{aligned}\dot{V}_2 &= \dot{V}_1 + \mathbf{e}_2^T\left(\mathbf{u}(t) - \mathbf{C}_0(\mathbf{x}_1, \mathbf{x}_2)\mathbf{x}_2(t) - \mathbf{G}_0(\mathbf{x}_1) - \Delta(t)\right. \\ &\quad \left. - \mathbf{M}(\mathbf{x}_1)\dot{\boldsymbol{\alpha}}_1 + \mathbf{C}(\mathbf{x}_1, \mathbf{x}_2)\mathbf{e}_2\right) \\ &= -\mathbf{e}_z^T\mathbf{K}_{10}\mathbf{e}_z - \mathbf{e}_z^T\mathbf{K}_{11}\mathbf{e}_z^{\beta_2} - \mathbf{e}_2^T\mathbf{K}_{20}\mathbf{e}_2 - \mathbf{e}_2^T\mathbf{K}_{21}\mathbf{e}_2^{\beta_2} \\ &\quad + \mathbf{e}_2^T\mathbf{C}_0(\mathbf{x}_1, \mathbf{x}_2)\boldsymbol{\alpha}_1 + \mathbf{e}_2^T\mathbf{G}_0(\mathbf{x}_1) + \mathbf{e}_2^T\mathbf{M}_0(\mathbf{x}_1)\dot{\boldsymbol{\alpha}}_1 \\ &\quad - \mathbf{e}_2^T\mathbf{C}_0(\mathbf{x}_1, \mathbf{x}_2)\mathbf{x}_2 - \mathbf{e}_2^T\mathbf{G}_0(\mathbf{x}_1) - \mathbf{e}_2^T\boldsymbol{\Delta}(t) \\ &\quad - \mathbf{e}_2^T\mathbf{M}(\mathbf{x}_1)\dot{\boldsymbol{\alpha}}_1 + \mathbf{e}_2^T\mathbf{C}(\mathbf{x}_1, \mathbf{x}_2)\mathbf{e}_2 \\ &= -\mathbf{e}_z^T\mathbf{K}_{10}\mathbf{e}_z - \mathbf{e}_2^T(\mathbf{K}_{20} - \Delta\mathbf{C}(\mathbf{x}_1, \mathbf{x}_2))\mathbf{e}_2 - \mathbf{e}_z^T\mathbf{K}_{11}\mathbf{e}_z^{\beta_2} \\ &\quad - \mathbf{e}_2^T\mathbf{K}_{21}\mathbf{e}_2^{\beta_2} - \mathbf{e}_2^T(\boldsymbol{\Delta}(t) + \Delta\mathbf{M}(\mathbf{x}_1)\dot{\boldsymbol{\alpha}}_1)\end{aligned} \tag{45}$$

Based on Young's inequality, $-\mathbf{e}_2^T\boldsymbol{\Delta}(t) \le \frac{1}{2}\mathbf{e}_2^T\mathbf{e}_2 + \frac{1}{2}\boldsymbol{\Delta}^T(t)\boldsymbol{\Delta}(t)$, $-\mathbf{e}_2^T\Delta\mathbf{M}(\mathbf{x}_1)\dot{\boldsymbol{\alpha}}_1 \le \frac{1}{2}\mathbf{e}_2^T\mathbf{e}_2 + \frac{1}{2}\dot{\boldsymbol{\alpha}}_1^T\Delta\mathbf{M}^T\Delta\mathbf{M}\dot{\boldsymbol{\alpha}}_1$ and the Lemma 2 in [38], the differential Lyapunov function is represented as follows:

$$\dot{V}_2 \le -\mathbf{e}_z^T\mathbf{K}_{10}\mathbf{e}_z - \mathbf{e}_2^T(\mathbf{K}_{20} - \Delta\mathbf{C}(\mathbf{x}_1, \mathbf{x}_2) - \mathbf{I}_{n\times n})\mathbf{e}_2$$

$$- \mathbf{e}_z^T \mathbf{K}_{11} \mathbf{e}_z^{\beta_2} - \mathbf{e}_2^T \mathbf{K}_{21} \mathbf{e}_2^{\beta_2} + \frac{1}{2} \boldsymbol{\Delta}^T (t) \boldsymbol{\Delta} (t) + \frac{1}{2} \dot{\boldsymbol{\alpha}}_1^T \Delta \mathbf{M}^T \Delta \mathbf{M} \dot{\boldsymbol{\alpha}}_1 \leq -\kappa_1 V_2 - \kappa_2 V_2^{\frac{1+\beta_2}{2}} + \delta_0 \tag{46}$$

where

$$\kappa_1 = \min \left(\lambda_{\min} (\mathbf{K}_{10}), \lambda_{\min} \left(\left(\mathbf{K}_{20} - \Delta \mathbf{C} (x_1, x_2) - \frac{1}{2} \mathbf{I}_{n \times n} \right) \mathbf{M}^{-1} \right) \right);$$

$$\kappa_2 = \min \left(\lambda_{\min} (\mathbf{K}_{11}), \lambda_{\min} \left(\mathbf{K}_{21} \mathbf{M}^{-\frac{1+\beta_2}{2}} \right) \right);$$

$$\delta_0 = \frac{1}{2} \max \left(\boldsymbol{\Delta}^T (t) \boldsymbol{\Delta} (t) + \dot{\boldsymbol{\alpha}}_1^T \Delta \mathbf{M}^T \Delta \mathbf{M} \dot{\boldsymbol{\alpha}}_1 \right).$$

There exists a scalar $0 < \varphi_0 < 1$ so that the differential Lyapunov function (46) can be represented in two cases. In the first case, $V_2 > \frac{\delta_0}{(1-\varphi_0)\kappa_1}$, its result yields

$$\begin{aligned} \dot{V}_2 &\leq -\varphi_0 \kappa_1 V_2 - (1 - \varphi_0) \kappa_1 V_2 - \kappa_2 V_2^{\frac{1+\beta_2}{2}} + \delta_0 \\ &\leq -\varphi_0 \kappa_1 V_2 - \kappa_2 V_2^{\frac{1+\beta_2}{2}} \end{aligned} \tag{47}$$

Based on Lemma 1 in [39], the errors are driven into the region $\mathbf{e} = \begin{bmatrix} \mathbf{e}_z^T & \mathbf{e}_2^T \end{bmatrix}^T \in \left\{ V_2 \leq \frac{\delta_0}{(1-\varphi_0)\kappa_1} \right\}$ in a finite time given as

$$T_r \leq t_0 + \frac{2}{\varphi_0 (1 - \beta_2)} \ln \frac{\varphi_0 \kappa_1 V_2^{\frac{1+\beta_2}{2}} (e (t_0)) + \kappa_2}{\kappa_2} \tag{48}$$

In the second case, $V_2^{\frac{1+\beta}{2}} > \frac{\delta_0}{(1-\varphi_0)\kappa_2}$, its result is presented as

$$\begin{aligned} \dot{V}_2 &\leq {}_2 - \kappa_1 V_2 - \varphi_0 \kappa_2 V_2^{\frac{1+\beta_2}{2}} - (1 - \varphi_0) \kappa_2 V_2^{\frac{1+\beta_2}{2}} + \delta_0 \\ &\leq -\kappa_1 V_2 - \varphi_0 \kappa_2 V_2^{\frac{1+\beta_2}{2}} \end{aligned} \tag{49}$$

By a similar analysis, the errors are driven into the region $\mathbf{e} \in \left\{ V_2^{\frac{1+\beta}{2}} \leq \frac{\delta_0}{(1-\varphi_0)\kappa_2} \right\}$ within a finite time which is presented as

$$T_r \leq t_0 + \frac{2}{\kappa_1 (1 - \beta_2)} \ln \frac{\kappa_1 V_2^{\frac{1+\beta_2}{2}} (e (t_0)) + \varphi_0 \kappa_2}{\varphi_0 \kappa_2} \tag{50}$$

From (46), (48) and (50), **Theorem 2** is proven.

APPENDIX C

In order to prove theorem 3, the Lyapunov function is selected based on (36) and (42) as follows:

$$V = V_0 + V_2 = \frac{1}{2} \boldsymbol{\sigma}^T \mathbf{P} \boldsymbol{\sigma} + \frac{1}{2} \mathbf{e}_z^T \mathbf{e}_z + \frac{1}{2} \mathbf{e}_2^T \mathbf{M} \mathbf{e}_2 \tag{51}$$

The differential Lyapunov function is presented as

$$\begin{aligned} \dot{V} &= \boldsymbol{\sigma}^T \mathbf{P} \dot{\boldsymbol{\sigma}} + \mathbf{e}_z^T \dot{\mathbf{e}}_z + \mathbf{e}_2^T \mathbf{M} \dot{\mathbf{e}}_2 + \frac{1}{2} \mathbf{e}_2^T \dot{\mathbf{M}} (\mathbf{x}_1) \mathbf{e}_2 \\ &\leq -\mathbf{e}_z^T \mathbf{K}_{10} \mathbf{e}_z - \mathbf{e}_z^T \mathbf{K}_{11} \mathbf{e}_z^{\beta_2} \\ &\quad + \mathbf{e}_z^T \boldsymbol{\Phi} \mathbf{e}_2 + \left(-\left(\gamma - \frac{c \lambda_{\max} (\mathbf{P})}{\gamma} \right) \|\boldsymbol{\sigma}\|_2 \right. \\ &\quad \left. + \frac{\bar{\delta}}{\gamma^2} \lambda_{\max} (\mathbf{P}) \right) \|\boldsymbol{\sigma}\|_2 + \mathbf{e}_2^T (\mathbf{u} (t) \\ &\quad - \mathbf{C}_0 (\mathbf{x}_1, \mathbf{x}_2) \mathbf{x}_2 - \mathbf{G}_0 (\mathbf{x}_1 - \boldsymbol{\Delta} (t) - \mathbf{M}_0 (\mathbf{x}_1) \dot{\boldsymbol{\alpha}}_1 \\ &\quad + \mathbf{C} (\mathbf{x}_1, \mathbf{x}_2) \mathbf{e}_2) \\ &\leq \left(-\left(\gamma - \frac{c \lambda_{\max} (\mathbf{P})}{\gamma} \right) \|\boldsymbol{\sigma}\|_2 + \frac{\bar{\delta}}{\gamma^2} \lambda_{\max} (\mathbf{P}) \right) \|\boldsymbol{\sigma}\|_2 \\ &\quad - \mathbf{e}_z^T \mathbf{K}_{10} \mathbf{e}_z - \mathbf{e}_z^T \mathbf{K}_{11} \mathbf{e}_z^{\beta_2} - \mathbf{e}_2^T \mathbf{K}_{20} \hat{\mathbf{e}}_2 - \mathbf{e}_2^T \mathbf{K}_{21} \hat{\mathbf{e}}_2^{\beta_2} \\ &\quad + c \mathbf{e}_2^T |\boldsymbol{\sigma}| + \mathbf{e}_2^T \mathbf{M}_0 (\mathbf{x}_1) \tilde{\mathbf{x}}_3 - \mathbf{e}_2^T \Delta \mathbf{M} (\mathbf{x}_1) \dot{\boldsymbol{\alpha}}_1 \end{aligned} \tag{52}$$

Based on Young's inequality, $\mathbf{e}_2^T |\boldsymbol{\sigma}| \leq \frac{1}{2} \mathbf{e}_2^T \mathbf{e}_2 + \frac{1}{2} \boldsymbol{\sigma}^T \boldsymbol{\sigma}$, $\mathbf{e}_2^T \mathbf{M}_0 (\mathbf{x}_1) \tilde{\mathbf{x}}_3 \leq \frac{1}{2} \mathbf{e}_2^T \mathbf{M}_0^T (\mathbf{x}_1) \mathbf{M}_0 (\mathbf{x}_1) \mathbf{e}_2 + \frac{1}{2} \tilde{\mathbf{x}}_3^T \tilde{\mathbf{x}}_3$, the differential Lyapunov function (51) is rewritten as follows

$$\begin{aligned} \dot{V} &\leq -\left(\gamma - \frac{c \lambda_{\max} (\mathbf{P})}{\gamma} - \frac{c}{2} \right) \|\boldsymbol{\sigma}\|_2^2 - \mathbf{e}_z^T \mathbf{K}_{10} \mathbf{e}_z \\ &\quad - \mathbf{e}_z^T \mathbf{K}_{11} \mathbf{e}_z^{\beta_2} - \mathbf{e}_2^T \mathbf{K}_{21} \hat{\mathbf{e}}_2^{\beta_2} \\ &\quad - \mathbf{e}_2^T \left(\mathbf{K}_{20} - \frac{c \mathbf{I}_{n \times n} + \lambda_{\max} \left(\mathbf{M}_0^T (\mathbf{x}_1) \mathbf{M}_0 (\mathbf{x}_1) \right)}{2} \right) \mathbf{e}_2 \\ &\quad + \frac{\bar{\delta}}{\gamma^2} \lambda_{\max} (\mathbf{P}) \|\boldsymbol{\sigma}\|_2 + \frac{1}{2} \tilde{x}_3^T \tilde{x}_3 \\ &\leq -\left(\gamma - \frac{c \lambda_{\max} (\mathbf{P})}{\gamma} - \frac{c}{2} \right) \|\boldsymbol{\sigma}\|_2^2 - \mathbf{e}_z^T \mathbf{K}_{10} \mathbf{e}_z \\ &\quad + \frac{\bar{\delta}}{\gamma^2} \lambda_{\max} (\mathbf{P}) \|\boldsymbol{\sigma}\|_2 \\ &\quad + \frac{1}{2} \tilde{\mathbf{x}}_3^T \tilde{\mathbf{x}}_3 \\ &\quad - e_2^T \left(\mathbf{K}_{20} - \frac{c \mathbf{I}_{n \times n} + \lambda_{\max} \left(\mathbf{M}^T (\mathbf{x}_1) \mathbf{M} (\mathbf{x}_1) \right)}{2} \right) \mathbf{e}_2 \\ &\leq -\kappa V + \Delta_V \end{aligned} \tag{53}$$

where $\kappa = \min$
$\left(\lambda_{\min} \left(\left(\mathbf{K}_{20} - \frac{c \mathbf{I}_{n \times n} + \lambda_{\max} \left(\mathbf{M}_0^T (\mathbf{x}_1) \mathbf{M}_0 (\mathbf{x}_1) \right)}{2} \right) \mathbf{M}^{-1} \right), \right.$
$\left. \mathbf{K}_{10}, \left(\gamma - \frac{c \lambda_{\max} (\mathbf{P})}{\gamma} - \frac{c}{2} \right) \lambda_{\max} \left(\mathbf{P}^{-1} \right) \right),$
$\Delta_V = \max \left(\frac{\bar{\delta}}{\gamma^2} \lambda_{\max} (\mathbf{P}) \|\boldsymbol{\sigma}\|_2 + \frac{1}{2} \tilde{\mathbf{x}}_3^T \tilde{\mathbf{x}}_3 \right).$

From (53), the parameters of the observer and control should be selected to satisfy the below conditions:

$$\begin{aligned} &\gamma - \frac{c \lambda_{\max} (\mathbf{P})}{\gamma} - \frac{c}{2} > 0 \\ &\times \lambda_{\min} \left(\left(\mathbf{K}_{20} - \frac{c_2 \mathbf{I}_{n \times n} + \lambda_{\max} \left(\mathbf{M}_0^T (\mathbf{x}_1) \mathbf{M}_0 (\mathbf{x}_1) \right)}{2} \right) \right. \\ &\left. \times \mathbf{M}^{-1} \right) > 0 \end{aligned} \tag{54}$$

Then, we can affirm that the system (24) is uniformly ultimately bounded [40] with the control laws in (33) and (34), and the observer in (17). Furthermore, based on nonlinear transformation in Section II. B, the output performances are bounded by predefined constraints. Theorem 3 is proven.

REFERENCES

[1] H. I. Krebs, M. Ferraro, S. P. Buerger, M. J. Newbery, A. Makiyama, M. Sandmann, D. Lynch, B. T. Volpe, and N. Hogan, "Rehabilitation robotics: Pilot trial of a spatial extension for MIT-MANUS," *J. NeuroEng. Rehabil.*, vol. 1, no. 1, p. 5, 2004.

[2] B. Whitsell and P. Artemiadis, "Physical human–robot interaction (pHRI) in 6 DOF with asymmetric cooperation," *IEEE Access*, vol. 5, pp. 10834–10845, 2017.

[3] Z. Chen, F. Huang, W. Chen, J. Zhang, W. Sun, J. Chen, J. Gu, and S. Zhu, "RBFNN-based adaptive sliding mode control design for delayed nonlinear multilateral telerobotic system with cooperative manipulation," *IEEE Trans. Ind. Informat.*, vol. 16, no. 2, pp. 1236–1247, Feb. 2020.

[4] L. Edalatia, A. Khaki, M. Aliyari, and A. Moarefianpoura, "Adaptive fuzzy dynamic surface control of nonlinear systems with input saturation and time-varying output constraints," *Mech. Syst. Signal Process.*, vol. 100, pp. 311–329, Feb. 2018.

[5] Y. Zhang, S. Li, S. Kadry, and B. Liao, "Recurrent neural network for kinematic control of redundant manipulators with periodic input disturbance and physical constraints," *IEEE Trans. Cybern.*, vol. 49, no. 12, pp. 4194–4205, Dec. 2019.

[6] Y. Qiu, X. Liang, Z. Dai, J. Cao, and Y. Chen, "Backstepping dynamic surface control for a class of non-linear systems with time-varying output constraints," *IET Control Theory Appl.*, vol. 9, no. 15, pp. 2312–2319, Oct. 2015.

[7] K. P. Tee, S. S. Ge, and E. H. Tay, "Barrier Lyapunov functions for the control of output-constrained nonlinear systems," *Automatica*, vol. 45, no. 4, pp. 918–927, Apr. 2009.

[8] W. C. Meng, Q. M. Yang, and Y. X. Sun, "Adaptive neural control of nonlinear MIMO systems with time-varying output constraints," *IEEE Trans. Neural Netw. Learn. Syst.*, vol. 26, no. 5, pp. 1074–1085, May 2015.

[9] K. P. Tee, B. Ren, and S. S. Ge, "Control of nonlinear systems with time-varying output constraints," *Automatica*, vol. 47, no. 11, pp. 2511–2516, Nov. 2011.

[10] W. Wang and S. Tong, "Adaptive fuzzy containment control of nonlinear strict-feedback systems with full state constraints," *IEEE Trans. Fuzzy Syst.*, vol. 27, no. 10, pp. 2024–2038, Oct. 2019.

[11] Y. Wu, R. Huang, X. Li, and S. Liu, "Adaptive neural network control of uncertain robotic manipulators with external disturbance and time-varying output constraints," *Neurocomputing*, vol. 323, pp. 108–116, Jan. 2019.

[12] Y.-J. Liu, S. Lu, and S. Tong, "Neural network controller design for an uncertain robot with time-varying output constraint," *IEEE Trans. Syst., Man, Cybern., Syst.*, vol. 47, no. 8, pp. 2060–2068, Aug. 2017.

[13] C. P. Bechlioulis and G. A. Rovithakis, "Robust adaptive control of feedback linearizable MIMO nonlinear systems with prescribed performance," *IEEE Trans. Autom. Control*, vol. 53, no. 9, pp. 2090–2099, Oct. 2008.

[14] Z. Zhao and C. K. Ahn, "Boundary output constrained control for a flexible beam system with prescribed performance," *IEEE Trans. Syst., Man, Cybern., Syst.*, vol. 51, no. 8, pp. 4650–4658, Aug. 2021.

[15] H. Ma, Q. Zhou, H. Li, and R. Lu, "Adaptive prescribed performance control of a flexible-joint robotic manipulator with dynamic uncertainties," *IEEE Trans. Cybern.*, early access, Aug. 16, 2021, doi: 10.1109/TCYB.2021.3091531.

[16] Y.-J. Liu and H. Chen, "Adaptive sliding mode control for uncertain active suspension systems with prescribed performance," *IEEE Trans. Syst., Man, Cybern., Syst.*, vol. 51, no. 10, pp. 6414–6422, Oct. 2021.

[17] J. Gu, R. Sun, and J. Chen, "Improved back-stepping control for nonlinear small UAV systems with transient prescribed performance design," *IEEE Access*, vol. 9, pp. 128786–128798, 2021.

[18] J.-X. Zhang and G.-H. Yang, "Fuzzy adaptive output feedback control of uncertain nonlinear systems with prescribed performance," *IEEE Trans. Cybern.*, vol. 48, no. 5, pp. 1342–1354, May 2018.

[19] C.-C. Wang and G.-H. Yang, "Neural network-based adaptive output feedback fault-tolerant control for nonlinear systems with prescribed performance," *Neurocomputing*, vol. 329, pp. 457–467, Feb. 2019.

[20] Q. Zhou, H. Li, L. Wang, and R. Lu, "Prescribed performance observer-based adaptive fuzzy control for nonstrict-feedback stochastic nonlinear systems," *IEEE Trans. Syst., Man, Cybern., Syst.*, vol. 48, no. 10, pp. 1747–1758, Oct. 2018.

[21] M. Wang and A. Yang, "Dynamic learning from adaptive neural control of robot manipulators with prescribed performance," *IEEE Trans. Syst., Man, Cybern., Syst.*, vol. 47, no. 8, pp. 2244–2255, Aug. 2017.

[22] J. Lee, P. H. Chang, and M. Jin, "Adaptive integral sliding mode control with time-delay estimation for robot manipulators," *IEEE Trans. Ind. Electron.*, vol. 64, no. 8, pp. 6796–6804, Aug. 2017.

[23] J. Na, Y. Li, Y. Huang, G. Gao, and Q. Chen, "Output feedback control of uncertain hydraulic servo systems," *IEEE Trans. Ind. Electron.*, vol. 67, no. 1, pp. 490–500, Jan. 2020.

[24] J. Han, "From PID to active disturbance rejection control," *IEEE Trans. Ind. Electron.*, vol. 56, no. 3, pp. 900–906, Mar. 2009.

[25] D.-T. Tran, T.-C. Do, and K.-K. Ahn, "Extended high gain observer-based sliding mode control for an electro-hydraulic system with a variant payload," *Int. J. Precis. Eng. Manuf.*, vol. 20, no. 12, pp. 2089–2100, Dec. 2019.

[26] L. Zhao, X. Liu, and T. Wang, "Trajectory tracking control for double-joint manipulator systems driven by pneumatic artificial muscles based on a nonlinear extended state observer," *Mech. Syst. Signal Process.*, vol. 122, pp. 307–320, May 2019.

[27] H. Yang, Y. Yu, Y. Yuan, and X. Fan, "Back-stepping control of two-link flexible manipulator based on an extended state observer," *Adv. Space Res.*, vol. 56, no. 10, pp. 2312–2322, 2015.

[28] D. T. Tran, M. Jin, and K. K. Ahn, "Nonlinear extended state observer based on output feedback control for a manipulator with time-varying output constraints and external disturbance," *IEEE Access*, vol. 7, pp. 156860–156870, 2019.

[29] V. Nguyen, C. Lin, S. Su, W. Sun, and M. J. Er, "Global finite time active disturbance rejection control for parallel manipulators with unknown bounded uncertainties," *IEEE Trans. Syst., Man, Cybern., Syst.*, vol. 51, no. 12, pp. 7838–7849, Dec. 2021.

[30] R. M. Murray, Z. Li, S. S. Sastry, and S. S. Sastry, *A Mathematical Introduction to Robotic Manipulation*. Boca Raton, FL, USA: CRC Press, 1994.

[31] F. L. Lewis, D. M. Dawson, and C. T. Abdallah, *Robot Manipulator Control: Theory and Practice*. Boca Raton, FL, USA: CRC Press, 2003.

[32] D. T. Tran and K. K. Ahn, "Finite-time fault-tolerant control for a robotic manipulator with output constraint and uncertainties," *IEEE Access*, vol. 9, pp. 146771–146782, 2021.

[33] Z.-L. Zhao and B.-Z. Guo, "A novel extended state observer for output tracking of MIMO systems with mismatched uncertainty," *IEEE Trans. Autom. Control*, vol. 63, no. 1, pp. 211–218, Jan. 2018.

[34] S. Yu, X. Yu, B. Shirinzadeh, and Z. Man, "Continuous finite-time control for robotic manipulators with terminal sliding mode," *Automatica*, vol. 41, no. 11, pp. 1957–1964, Nov. 2005.

[35] D.-T. Tran, H.-V.-A. Truong, and K. K. Ahn, "Adaptive backstepping sliding mode control based RBFNN for a hydraulic manipulator including actuator dynamics," *Appl. Sci.*, vol. 9, no. 6, p. 1265, 2019.

[36] G. Yang, J. Yao, and N. Ullah, "Neuroadaptive control of saturated nonlinear systems with disturbance compensation," *ISA Trans.*, vol. 122, pp. 49–62, Mar. 2022.

[37] Q. Guo, Y. Zhang, B. Celler, and S. Su, "Backstepping control of electro-hydraulic system based on extended-state-observer with plant dynamics largely unknown," *IEEE Trans. Ind. Electron.*, vol. 63, no. 11, pp. 6909–6920, Nov. 2016.

[38] X. Huang, W. Lin, and B. Yang, "Global finite-time stabilization of a class of uncertain nonlinear systems," *Automatica*, vol. 41, no. 5, pp. 881–888, May 2005.

[39] J. Yu, P. Shi, and L. Zhao, "Finite-time command filtered backstepping control for a class of nonlinear systems," *Automatica*, vol. 92, pp. 173–180, Jun. 2018.

[40] A.-C. Huang and M.-C. Chien, *Adaptive Control of Robot Manipulators: A Unified Regressor-Free Approach*. Singapore: World Scientific, 2010.

DUC THIEN TRAN (Member, IEEE) received the B.S and M.S. degrees from the Department of Electrical Engineering, Ho Chi Minh City University of Technology, Vietnam, in 2010 and 2013, respectively, and the Ph.D. degree from the University of Ulsan, in 2020.

He works as a Lecturer with the Department of Automatic Control, Ho Chi Minh City University of Technology and Education (HCMUTE), Vietnam. His research interests include robotics, variable stiffness systems, fluid power control, disturbance observer, nonlinear control, adaptive control, fault tolerant control, and intelligent technique.

HOAI VU ANH TRUONG received the B.S. degree in mechanical engineering from the Ho Chi Minh City University of Technology, Ho Chi Minh City, Vietnam, in 2015, and the Ph.D. degree in mechanical and automotive engineering from the University of Ulsan, Ulsan, South Korea, in 2021.

He is currently a Postdoctoral Researcher with the mechanical and automotive engineering, University of Ulsan. His research interests include renewable energy, energy conversion systems, energy management for hybrid power sources, advanced control and intelligent control for nonlinear systems, nonlinear observer, fault-tolerant control, electro-hydraulic systems, and robotic manipulator.

MAOLIN JIN (Senior Member, IEEE) received the B.S. degree in material science and mechanical engineering from the Yanbian University of Science and Technology, Jilin, China, in 1999, and the M.S. and Ph.D. degrees in mechanical engineering from KAIST, Daejeon, South Korea, in 2004 and 2008, respectively.

He was a Postdoctoral Researcher at the Mechanical Engineering Research Institute, KAIST, in 2008. From November 2008 to February 2016, he was a Senior Researcher with the Research Institute of Industrial Science and Technology, Pohang, South Korea. He is currently a Director and a Chief Researcher with the Human-Centered Robotics Center of the KIRO, Pohang. His research interests include robust control of nonlinear plants, time-delay control, robot motion control, electro-hydraulic actuators, winding machines, collaborative robots, disaster robotics, and factory automation.

KYOUNG KWAN AHN (Senior Member, IEEE) received the B.S. degree from the Department of Mechanical Engineering, Seoul National University, in 1990, the M.Sc. degree in mechanical engineering from the Korea Advanced Institute of Science and Technology, in 1992, and the Ph.D. degree from the Tokyo Institute of Technology, in 1999.

He is currently a Professor with the School of Mechanical Engineering, University of Ulsan, Ulsan, South Korea. His research interests include the design and control of smart actuator using the smart material, fluid power control and active damping control, and renewable energy. He is an Editor of *IJCAS*, an Editorial Board of *Renewable Energy*, *Actuators*, and *Journal of Engineering*.